Egyptian Journal of Radiology and Nuclear Medicine

RESEARCH

Open Access

Magnetic resonance imaging with perfusion and diffusion in assessment of intra-spinal lesions

Maryam Hamdy Foaad*, Mohamed El Rakhawy and Mohamed Mohsen

Abstract

Background MRI is the imaging modality of choice in detecting and evaluating spinal lesions. However, advanced techniques as diffusion and perfusion studies can help more in differentiation between neoplastic and non-neoplastic lesions. Our study aimed to detect the role of diffusion and T2* perfusion weighted imaging in characterization of different spinal lesions by measuring the relative cerebral blood volume (rCBV) and apparent diffusion coefficient value (ADC) of all lesions, comparing perfusion of lesion in relation to normal cord and detection of diffusion pattern of each lesion by observing its signal intensity at diffusion images and ADC map.

Results Fifty patients were included in this study. Twenty-five patients were with non-neoplastic lesions and twenty-five patients were with neoplastic lesions. The cutoff value of rCBV was 1.2 in differentiation between neoplastic and non-neoplastic lesions with 92% sensitivity and 100% specificity. The cutoff value of ADC was 1 in differentiation between neoplastic and non-neoplastic lesions with 56% sensitivity and 80% specificity.

Conclusions Diffusion and perfusion weighted images help in differentiation between neoplastic and non-neoplastic spinal lesions.

Keywords MR diffusion, MR perfusion, Spinal lesions

Background

Spinal lesions have a wide variety of causes. Congenital causes include malformations of the spine which present since birth, often associated with spina bifida or scoliosis. Other causes are trauma, spinal cord infarction, chronic progressive myelopathy from arthritis or degenerative disk disease and autoimmune conditions (e.g., multiple sclerosis which produces spinal cord lesions in most of cases) [1].

Magnetic resonance imaging (MRI) is the imaging modality of choice in detecting and evaluating spinal tumors [2].

*Correspondence:
Maryam Hamdy Foaad
maryamhamdymh@gmail.com
Mansoura University, Mansoura 35511, Egypt

Spinal cord is examined only by a few advanced imaging techniques. Diffusion-weighted imaging has attracted clinical interest, while spectroscopy remains challenging to implement. MR perfusion studies of spinal cord lesions are limited to few related articles using dynamic susceptibility contrast (DSC) MR perfusion in the cervical region. However, the susceptibility artifacts and its semiquantitative nature limit this technique [3].

Dynamic susceptibility contrast perfusion on T2 weighted images exploits the regional susceptibility-induced signal loss by paramagnetic contrast (such as gadolinium-based compounds) [4]. Although both T2 (e.g., spin echo) and T2* (e.g., gradient-echo echo-planar) sequences can be used for this technique, the former requires larger contrast doses, which is why T2* approaches are more generally used [5].

Following images acquisition, the signal of a region is examined during the perfusion sequence, resulting in a signal intensity-time curve from which numerous parameters can be derived (e.g., rCBV, rCBF, MTT). These results can subsequently be utilized to construct regional perfusion color maps [6].

Diffusion-weighted MR imaging (DWI) increases the sensitivity and specificity of MRI in diagnosis and characterization of different spinal lesions, as it adds functional data obtained at the cellular level [7].

DWI is based on the random motion of water protons and is successfully used as an important diagnostic tool in the evaluation of different brain disorders. With its ability to detect altered water-proton mobility, it may also be useful for the evaluation of spinal disorders [8].

The aim of this study was to evaluate the role of dynamic contrast susceptibility T2* perfusion weighted and diffusion-weighted images in assessment and characterization of spinal lesions.

Methods

This prospective study was conducted in the Diagnostic and Interventional Radiology Department in our institution over the last 1.5 years (January 2021–June 2022). Informed written consents were obtained from all patients included in this study. Personal privacy was respected in all levels of this study.

Fifty patients with spinal lesions were included in this study. Inclusion criteria: any patient with spinal lesion detected by conventional MRI.

Exclusion criteria: patients having contraindication to MRI study (as those with cochlear implant, cardiac pacemaker, any metallic stent, claustrophobia and morbid obesity) and operated spinal lesions. Also, patients with vertebral lesions were excluded.

Pre- and post-contrast MRI was done with diffusion-weighted images, apparent diffusion coefficient value (ADC), and perfusion weighted images with analysis of the shape of the curve and the rCBV were analyzed. Pathology of neoplastic lesions was standard of our study.

The images were interpreted by two neuro-radiologists of 10 and 15 years' experience at the way of conjoint reading.

Examination of all patients was done by 1.5 T MRI (Philips Ingenia and Siemens Magnetom Aera).

Conventional MRI

MRI parameters included: FOV 250 mm, with 0.3 mm gap, 256 × 256 acquisition matrix and slice thickness of 1 mm. The sequences were as follow: For each sequence T2 spin echo (axial and sagittal) with 3500 ms TR, 88 ms TE, and acquisition time was 2 min 35 s. T1 spin echo (pre- and post-contrast sagittal imaging) with 640 ms TR, 10 ms TE, and acquisition time was 3 min 23 s.

Perfusion images

A single shot, gradient-echo, echo-planar imaging sequence was used to get dynamic T2* perfusion. During the first pass of contrast, FOV was 250 mm; TR/TE is 1520/32 ms; flip angle of 80°; matrix was 96 × 128; 10 mm thickness mid-sagittal slice; 50 scans. The contrast dose was calculated at 0.1 mmol/kg for 20 ml maximum. The total contrast was delivered with 5 ml/s rate.

A specific software package is used to assess the results of the post-processing (syngo neuro perfusion evaluation). The lesions and normal cord were used to produce perfusion mean curves in distinct regions of interest (ROIs). After that, comparison curves were created.

Diffusion-weighted imaging and ADC value

A single shot spin echo sequence which is multi-section with diffusion sensitivities of 0, 500, and 1000 s/mm^2 was used to acquire DW-MRI. The gradient of diffusion was done in three orthogonal directions consecutively (TR/TE was 1600/95 ms), and the matrix was (176 256), (6 mm) thickness, (1 mm) gap, (40 20) FOV, and a conventional spinal surface coil was used.

The ADC maps were generated automatically, and circular ROIs of 10 mm diameter were put in the lesion's center to produce ADC values with B values of 1000 s/mm^2.

Statistical analysis

The collected data were coded, processed, and analyzed using the SPSS (Statistical Package for Social Sciences) version 15 for Windows® (SPSS Inc, Chicago, IL, USA). Qualitative data was presented as number and percent. Comparison between groups was done by Chi-Square test. Quantitative data was tested for normality by Kolmogorov–Smirnov test. Normally distributed data was presented as mean ± SD. Nonparametric data was presented as min–max and median. Mann–Whitney test was used for comparison between groups. $P < 0.05$ was statistically significant.

Results

Fifty patients were included in this study. The classification of lesions was 25 neoplastic lesions and 25 non-neoplastic lesions. Twenty-seven patients were females while 23 were males, their age ranged from 11 to 71 years (mean age 40 years).

Twenty-four lesions were in the cervical region, 19 lesions were in the dorsal region and 7 lesions were in the lumbar region (Table 1).

Table 1 Distribution of lesions in relation to its location:

	Neoplastic $n=25$	Non neoplastic $n=25$	*P* value
Cervical *n* (%)	6 (24%)	18 (72%)	0.003*
Dorsal *n* (%)	14 (56%)	5 (20%)	
Lumbar *n* (%)	5 (20%)	2 (8%)	

*indicates statistically significant value

Table 2 Classification of lesions in relation to its nature

Neoplastic lesions *n* (%)	25 (50%)
Benign or low grade *n* (%)	14 (28%)
High grade *n* (%)	11 (22%)
Non neoplastic lesions *n* (%)	25 (50%)
Inflammatory *n* (%)	5 (10%)
Demyelinating *n* (%)	13 (26%)
Vascular *n* (%)	2 (4%)
Congenital *n* (%)	2 (4%)
Infection *n* (%)	3 (6%)

Most of non-neoplastic lesions were demyelinating (13), 5 lesions were inflammatory, 2 lesions were congenital syrinx, 2 lesions were vascular cavernoma and 3 lesions were infection. Neoplastic lesions were classified to benign/low-grade tumors and high grade tumors (Table 2).

All non-neoplastic lesions (100%) were hypo perfused in our study while only two cases (8%) of neoplastic lesions were hypo perfused, both were spinal metastasis. Twenty-three cases of neoplastic lesions were hyper perfused (11 lesions were high grade tumors, 14 were benign or low-grade tumors).

Perfusion imaging was done for 25 cases with spinal neoplastic lesions. We measured relative blood volume (rCBV) of the lesion in comparison to the normal spinal cord. Twenty-three cases of them showed increased rCBV in comparison to normal spinal cord (Figs. 1 and 2) except two lesions. The rCBV ratio was ranging from 0.79 to 4.3, with highest ratio seen in a case of spinal metastasis.

Perfusion was done in 25 non-neoplastic lesions. We measured rCBV in comparison to the normal spinal cord. All lesions showed decreased rCBV in comparison to normal spinal cord (Figs. 3 and 4) with median rCBV 0.35 ranging from 0.14 to 0.92.

Significant high rCBV ratio was found in neoplastic lesions unlike those of non-neoplastic etiology, which can help in differentiating between both categories (Table 3).

A cutoff value (1.2 for rCBV) had 92% sensitivity and 100% specificity in differentiation between neoplastic and non-neoplastic lesions. The area under curve was 0.980 which showed high statistically significance (*P* value < 0.001*) (Table 4).

In our study all benign and low-grade neoplastic lesions showed free diffusion (Fig. 5) while all high grade tumors showed restricted diffusion except one lesion. All non-neoplastic lesions showed free diffusion (Figs. 6 and 7) except one case which was diagnosed as chronic granulomatous lesion.

Median ADC value of neoplastic lesions (weather benign or malignant) was 1; its range was from 0.5 to 1.4.

Mean ADC value of benign and low-grade tumors was 1 while mean ADC value of high grade tumors was 0.7 (Table 3).

Median ADC value of non-neoplastic lesions was 1.2 ranging from 0.8 to 2.8. Median ADC value was higher in non-neoplastic and benign lesions than malignant neoplastic lesions.

Cutoff value of ADC (1) had 56% sensitivity and 80% specificity in differentiation between neoplastic and non-neoplastic lesions. The area under curve was 0.71 which was not statistically significant (*P* value 0.01*) (Table 5).

Cutoff value of ADC (1.05) had 100% sensitivity and 78.6% specificity in differentiation between benign or low-grade tumors and high grade tumors. The area under curve was 0.99 which was statistically significant (*P* value < 0.001*) (Table 6).

Discussion

MRI is the tool of choice for spinal cord imaging as it has high sensitivity for various intramedullary changes. DWI is a powerful tool for tissue investigation with conventional MR imaging. By sensitizing MR image to disturbance of random motion of water molecules in tissues, DWI provides unique insight into pathologic physiology [9].

Perfusion-weighted imaging (PWI) is a new tool which provides information about the hemodynamics of anatomic tissue or lesions and is mainly used in the assessment of disturbed cerebral hemodynamics. The mostly performed perfusion method is on the basis of T2* weighted dynamic susceptibility contrast-enhanced (DSC) MR echo-planar imaging approaches [10].

The most difficult part is calculating the rCBV ratio, which is an important measure in brain perfusion investigations. The rCBV ratio is estimated in the brain by dividing the CBV of a lesion by the CBV value of normal brain on the opposite side [11].

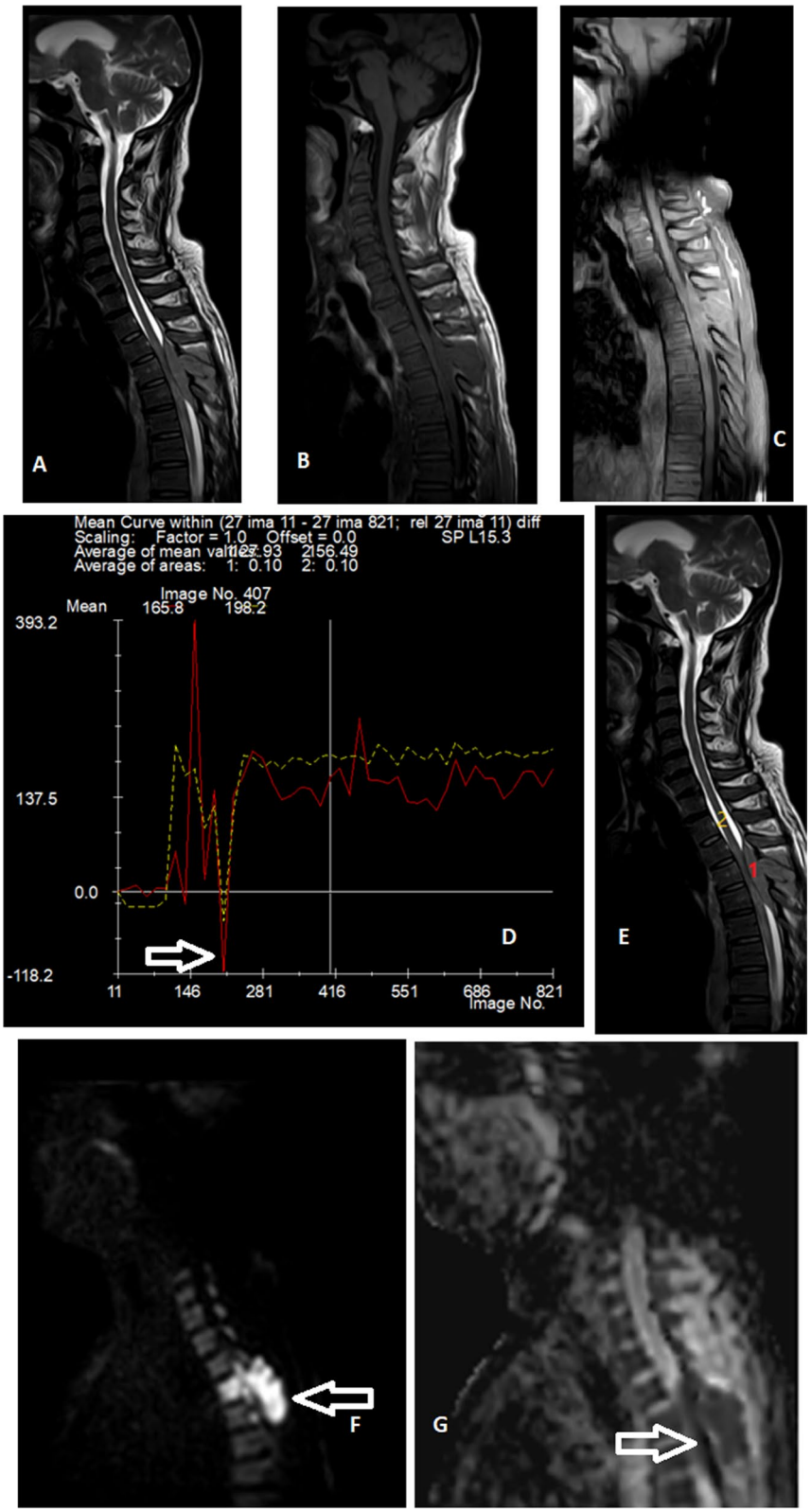

Fig. 1 46-y-old male was complaining of low back pain. T2 sagittal cervico-dorsal spine (**A**) shows extra-medullary soft tissue of isointense signal opposite D3-D7. Pre-contrast T1 (**B**) and post-contrast T1 (**C**) show intense enhancement of the lesion. **D** and **E** rCBV was measured in comparison to normal cord (yellow curve) and the curve shows hyper perfusion of the lesion (arrow to red curve). DWI at *b* value = 1000 **F** shows hyperintensity of the lesion (arrow) which looks hypointense at ADC map (arrow at **G**) denoting restricted diffusion. This lesion was diagnosed as spinal metastasis

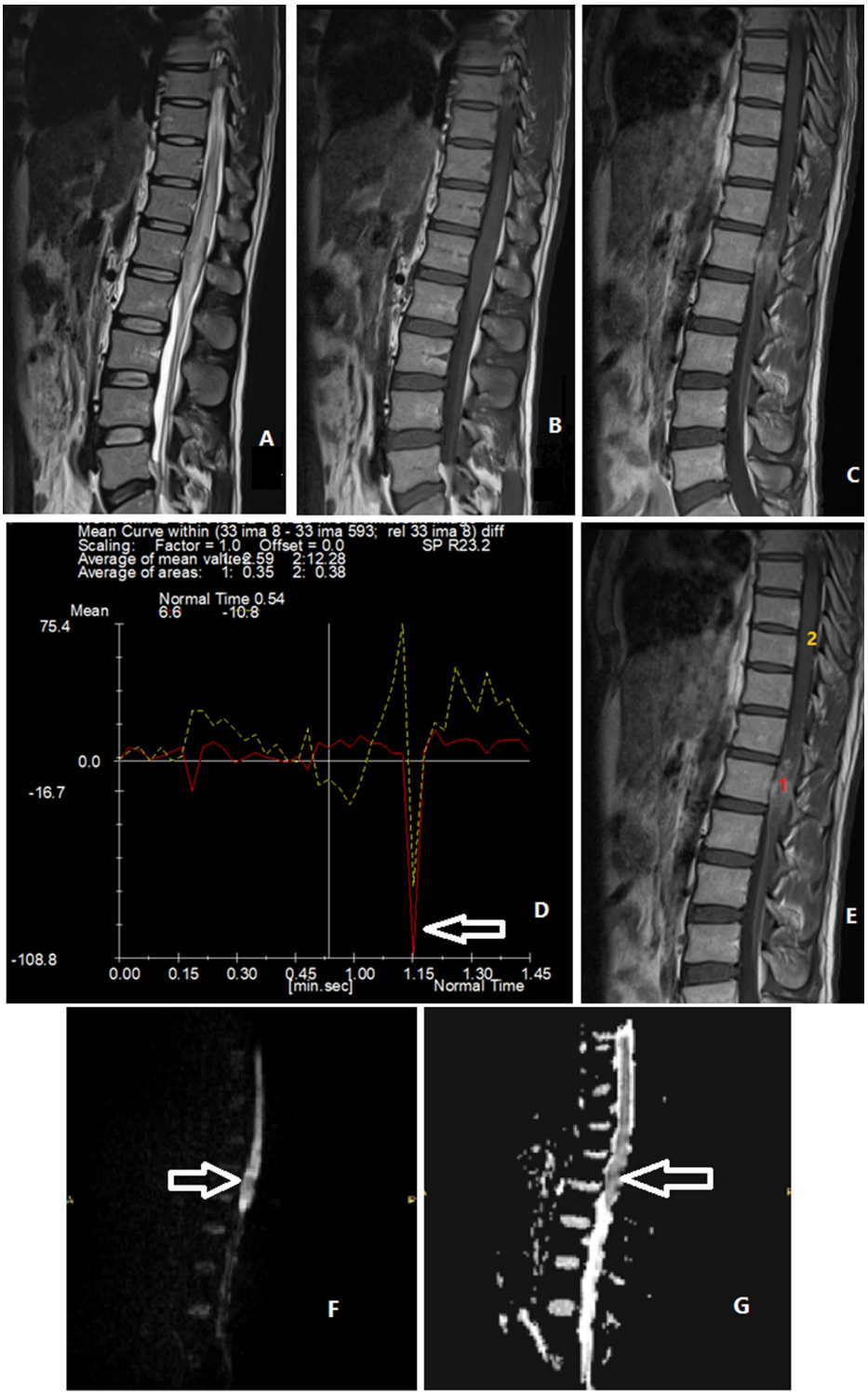

Fig. 2 29-year-old male presented with bilateral lower limb weakness. T2 sagittal dorso-lumbar spine (**A**) shows spinal cord expansion with high signal intensity. Pre-contrast T1 (**B**) and post-contrast T1 (**C**) show expansion of spinal cord with isointense signal and heterogeneous post-contrast enhancement. **D** and **E** rCBV was calculated in comparison to normal cord (yellow curve) and the curve shows hyper perfusion of the lesion (arrow to red curve). DWI at *b* value = 1000 (**F**) shows hyperintensity of the lesion (arrow) which looks also hyperintense at ADC map (arrow at **G**) denoting free diffusion. This lesion was diagnosed ependymoma (low grade)

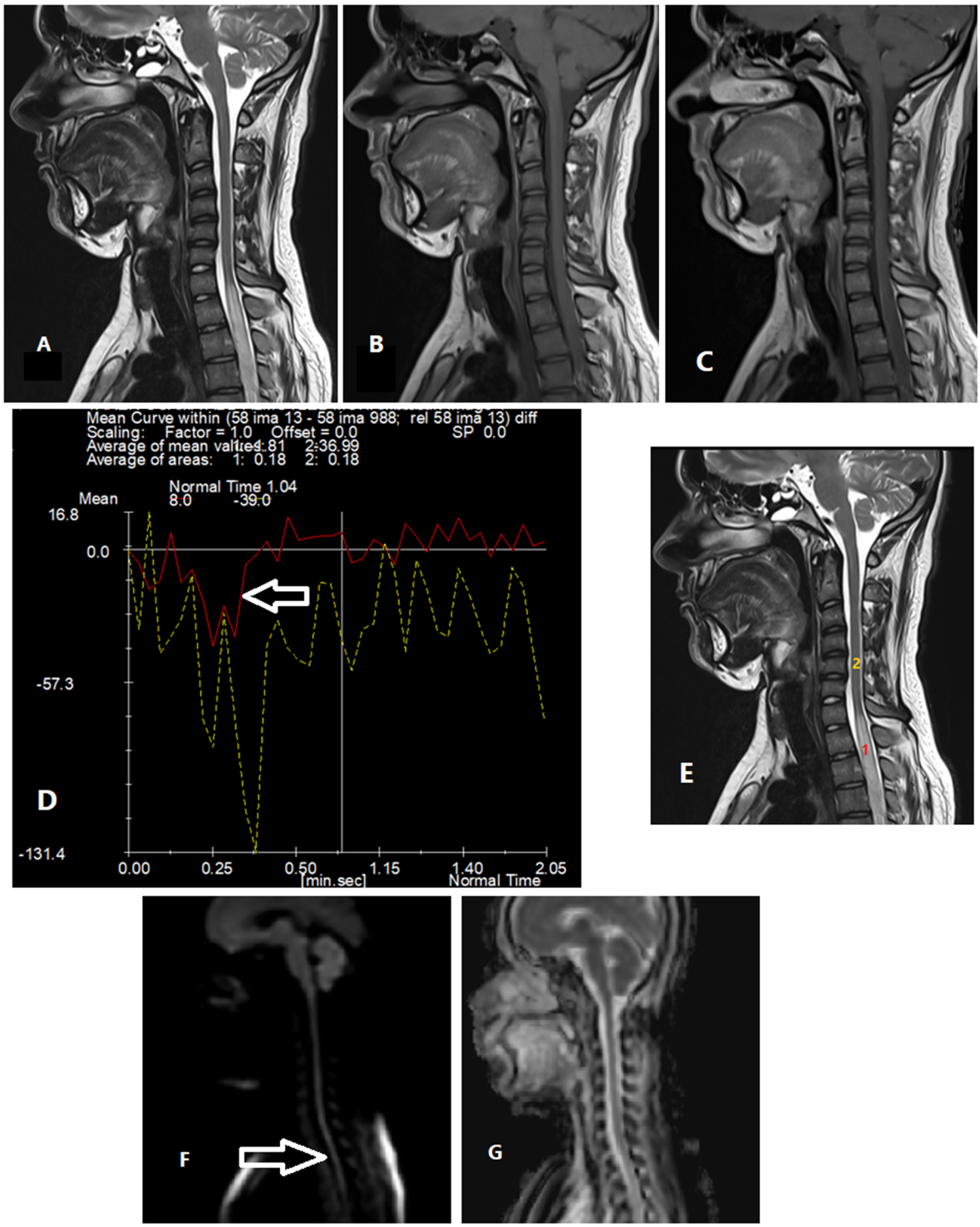

Fig. 3 18-year-old male presented with bilateral lower limb weakness. T2 sagittal cervico-dorsal spine (**A**) shows long segment of high signal intensity involving the cord opposite lower cervical and upper dorsal vertebrae. Pre-contrast T1 (**B**) and post-contrast T1 (**C**) show no significant post-contrast enhancement. **D** and **E** rCBV was calculated in comparison to normal cord (yellow curve) and the curve shows hypo perfusion of the lesion (arrow to red curve). DWI at *b* value = 1000 (**F**) shows no areas of high signal intensity of the lesion (arrow) which appears also at ADC map (**G**) denoting free diffusion. This lesion was diagnosed as neuromyelitis optica

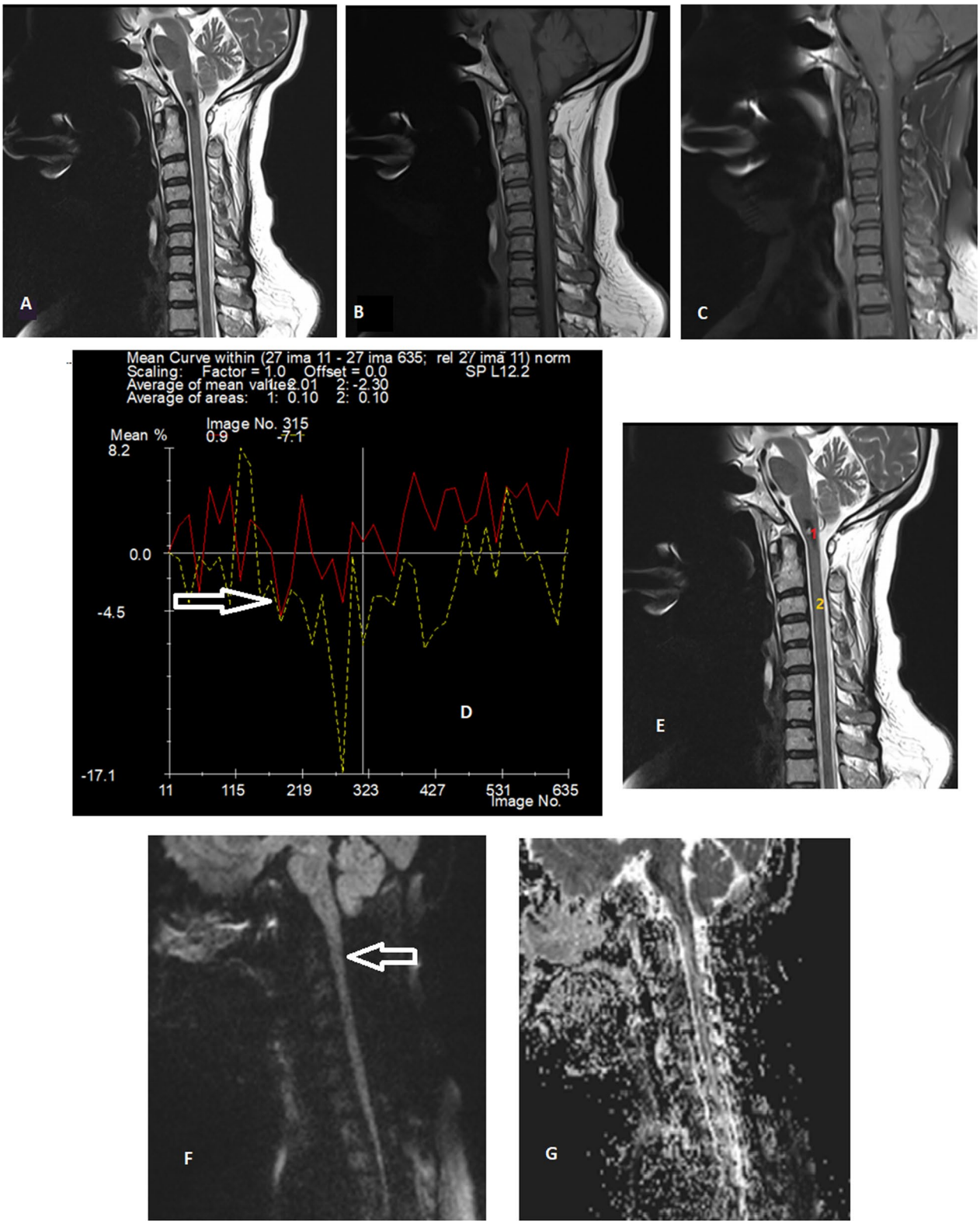

Fig. 4 54-year-old female presented with incidental cervico-medullary junction lesion. T2 sagittal cervical spine (**A**) shows small hyperintense lesion at cervico-medullary junction with peripheral hypointense rim. Pre-contrast T1 (**B**) and post-contrast T1 (**C**) show isointense lesion with no significant post-contrast enhancement. **D** and **E** rCBV was calculated in comparison to normal cord (yellow curve) and the curve shows hypo perfusion of the lesion (arrow to red curve). DWI at *b* value = 1000 (**F**) shows no areas of high signal intensity at site of lesion (arrow) which appears also at ADC map (**G**) denoting free diffusion. This lesion was diagnosed as cavernoma

Table 3 rCBV and ADC in relation to type of lesions

	Neoplastic *N* = 25	**Non neoplastic *N* = 25**	***P* value**
rCBV			
Median (IQR)	2 (1.8–2.5)	0.35 (0.28 -0.83)	< 0.001*
ADC value			
Median (IQR)	1 (0.7–1.2)	1.2 (1.1–1.3)	0.01*
	Benign and low-grade tumors	**High grade tumors**	
ADC value			
Mean ± SD	1 ± 0.15	0.7 ± 0.14	< 0.001*

*indicates statistically significant values

Table 4 Cutoff value, sensitivity and specificity of rCBV as a predictor of neoplastic lesions

	Cutoff point	**AUC**	***P* value**	**Sensitivity**	**Specificity**	**PPV**	**NPV**
rCBV	1.2	0.98	< 0.001*	92%	100%	100%	93%

*indicates statistically significant value

The acquisition plane decision is with controversy. The ROI is placed in the parenchyma of the normal appearing cerebral hemisphere for measurement of rCBV and ratio, and axial orientation is commonly employed for brain perfusion acquisitions [11].

Spinal intramedullary masses, on the other hand, can affect numerous segments and involve both the medulla and the cord. As a result, axial imaging will not detect the whole lesion which may result in underestimation of pathologic changes [12].

In our situations, we chose sagittal acquisition which can evaluate whole spinal lesion. This was in line with Liu et al. [11] suggestions.

Significant high rCBV was seen in neoplastic lesions more than non-neoplastic lesions in our study, which can help in differentiation of both lesions. This is similar to Al-AbdulJabbar et al. [13].

This also copes with Liu et al. [11] who found that spinal tumors have significantly higher perfusion than tumor like lesions depending on measurement of peak height of the bolus passage.

In our study all benign and low-grade neoplastic lesions showed free diffusion, while all high grade lesions showed restricted diffusion except one lesion. This copes with Hasan et al. [14] who found all spinal cord metastasis and high grade tumors exhibit restricted diffusion except one lesion of high grade glioma and found most low-grade tumors exhibit free diffusion.

All non-neoplastic lesions showed free diffusion in our study except one case which was diagnosed as chronic granulomatous lesion. We found that mean ADC value was higher in non-neoplastic and benign lesions than high grade neoplastic lesions, this copes with Hasan et al. [14].

Some limitation should be considered. Our study was confirmed on wide spectrum of spinal lesions so decrease sample size. Also, using two advanced MRI techniques trying to raise accuracy of MRI in characterization of spinal lesions increase time study resulting in patient discomfort.

Conclusions

Conventional MRI is the imaging modality of choice in detecting and evaluating spinal lesions but advanced imaging techniques as diffusion-weighted images and perfusion weighted images add more accuracy in differentiation and characterization.

(See figure on next page.)

Fig. 5 58-year-old male presented with bilateral lower limb weakness. T2 sagittal dorsal spine (**A**) shows well defined extradural lesion of isointense signal with intralesional foci of high signal intensity. Pre-contrast T1 (**B**) and post-contrast T1 (C) show homogenous post-contrast enhancement. **D** and **E** rCBV was calculated in comparison to normal cord (yellow curve) and the curve shows hyper perfusion of the lesion (arrow to red curve). DWI at *b* value = 1000 (**F**) shows central areas of high signal intensity within lesion. ADC map (**G**) shows iso- to hyperintense signal of whole lesion **(**arrow) denoting free diffusion. This lesion was diagnosed as benign extradural schwannoma

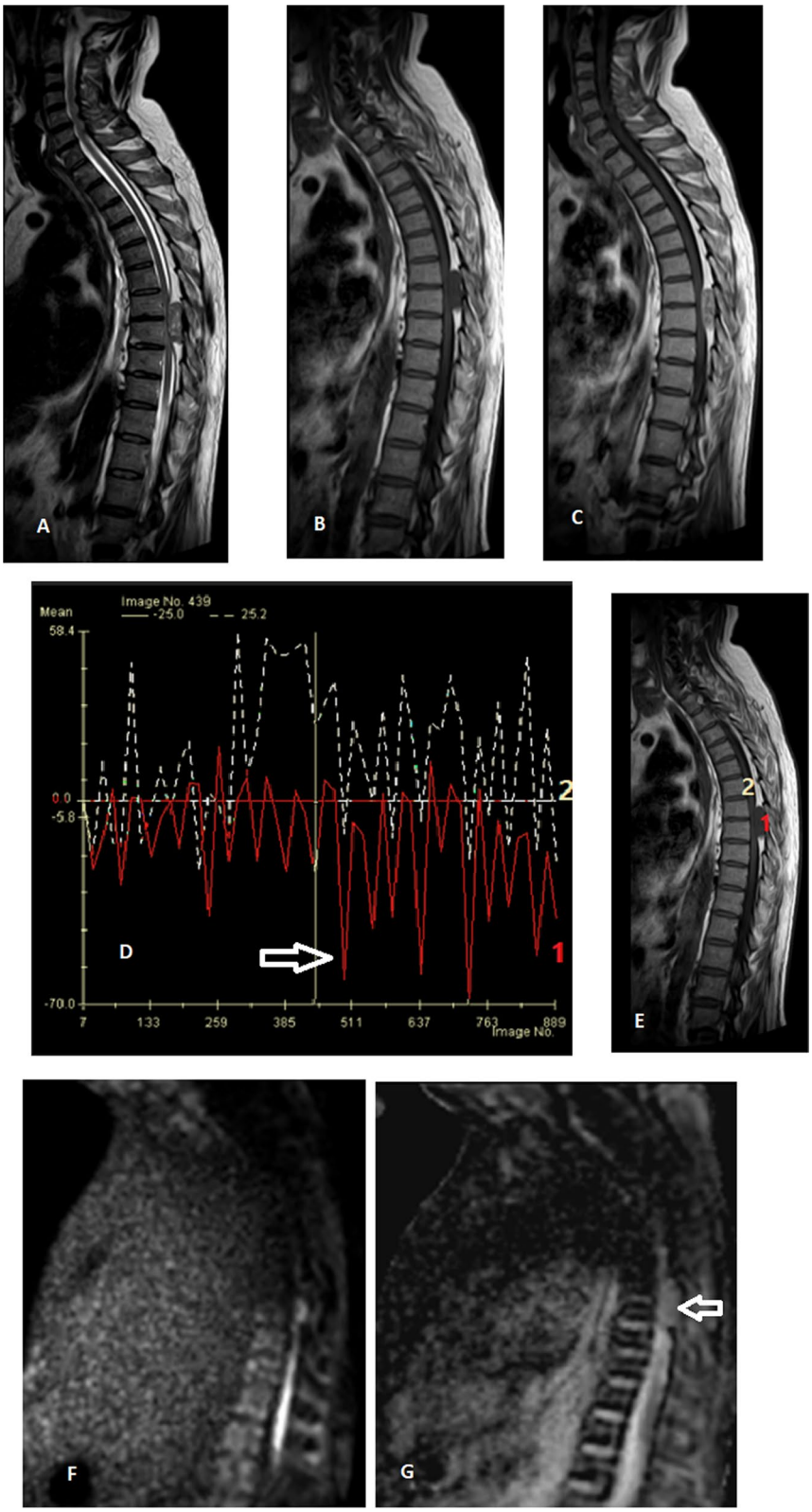

Fig. 5 (See legend on previous page.)

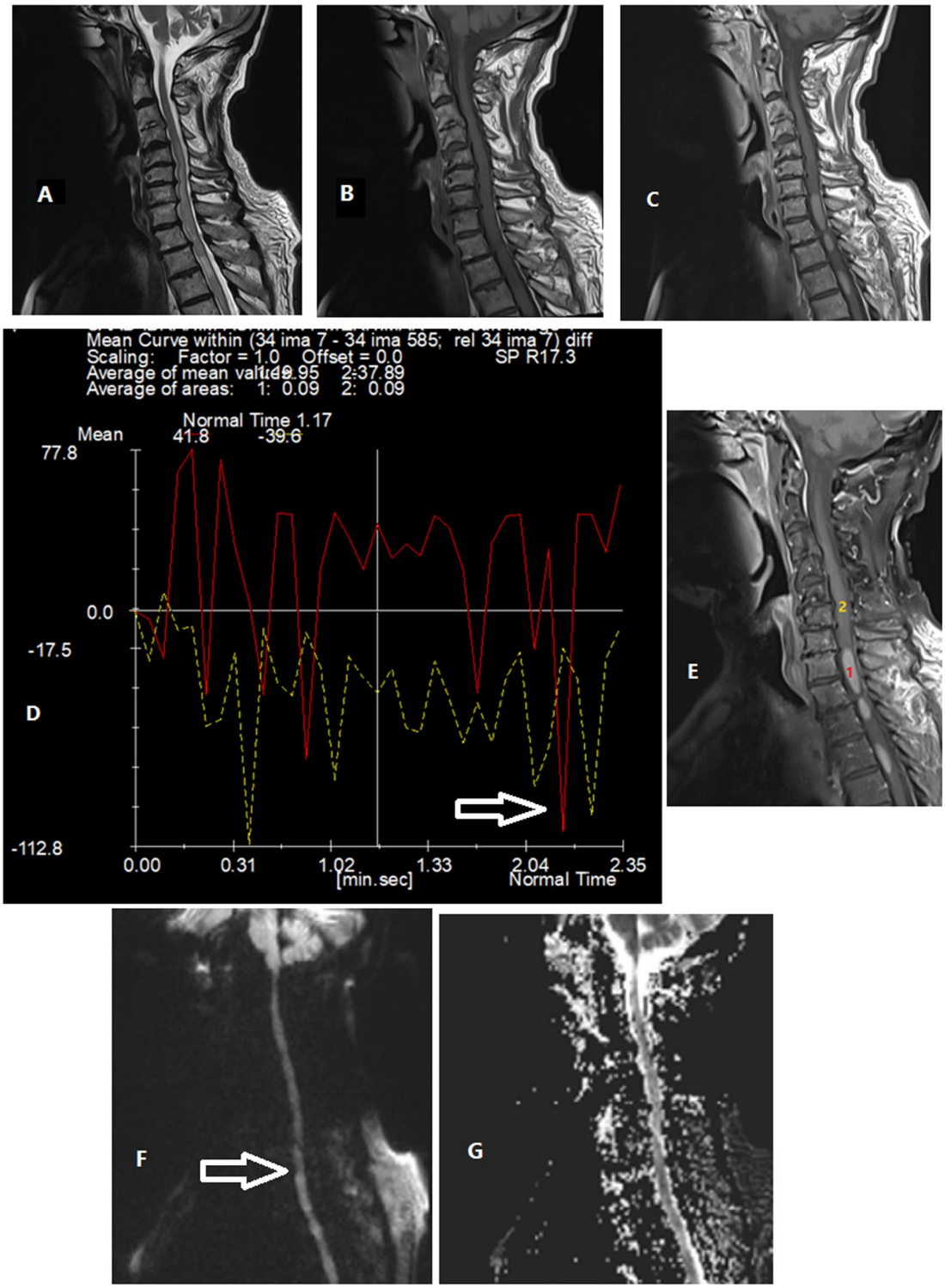

Fig. 6 71-year-old male presented with bilateral lower limb weakness and tingling sensation. T2 sagittal cervico-dorsal spine (**A**) shows interrupted areas of high signal intensity involving the cord opposite lower cervical and upper dorsal vertebrae. Pre-contrast T1 (**B**) and post-contrast T1 (**C**) show homogenous post-contrast enhancement. **D** and **E** rCBV was calculated in comparison to normal cord (yellow curve) and the curve shows hypo perfusion of the lesion (arrow to red curve). DWI at *b* value = 1000 (**F**) shows no areas of high signal intensity within cord at site of lesions (arrow) which appears also at ADC map (**G**) denoting free diffusion. This lesion was diagnosed as Para neoplastic myelitis

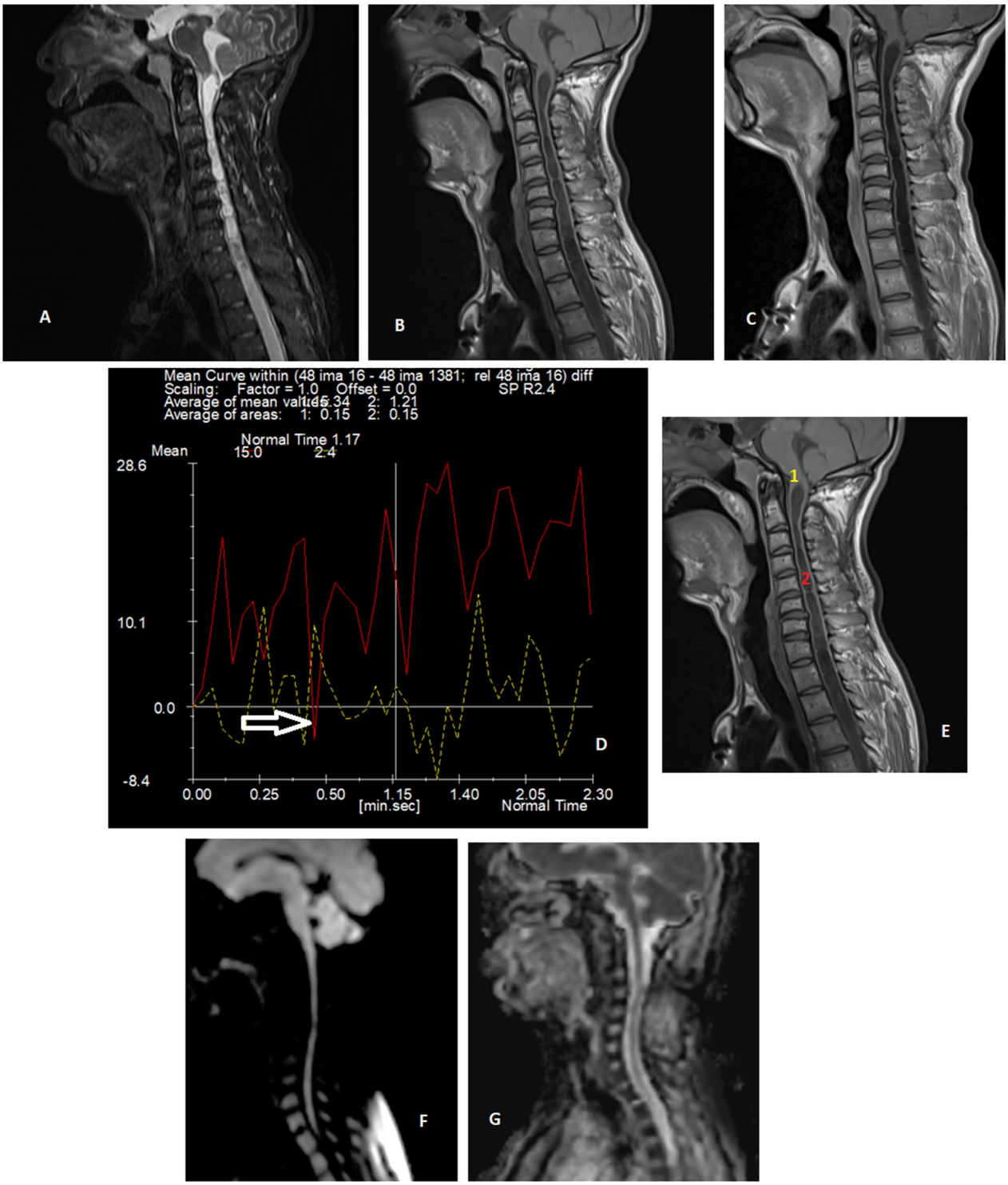

Fig. 7 23-year-old male presented with headache. T2 sagittal cervical spine (**A**) shows long segment of CSF signal intensity involving cervical and upper dorsal cord. Pre-contrast T1 (**B**) and post-contrast T1 (**C**) show CSF signal intensity of the lesion with no post-contrast enhancement. **D** and **E** rCBV was calculated in comparison to normal cord (yellow curve) and the curve shows hypo perfusion of the lesion (arrow to red curve). DWI at *b* value = 1000 (**F**) shows no areas of high signal intensity within cord at site of lesion which appears also at ADC map (**G**) denoting free diffusion. This lesion was diagnosed as syrinx associated with Chiari I malformation

Table 5 Cutoff value, sensitivity and specificity of ADC as a predictor of neoplastic lesions

	Cutoff point	AUC	*P* value	Sensitivity	Specificity	PPV	NPV
ADC	1	0.71	0.01*	56%	80%	74%	65%

*indicates statistically significant value

Table 6 Cutoff value, sensitivity and specificity of ADC as a predictor of high grade neoplastic lesions

	Cutoff point	AUC	*P* value	Sensitivity	Specificity	PPV	NPV
ADC	1.05	0.99	< 0.001*	100%	78.6%	78.6%	100%

*indicates statistically significant value

Abbreviations

MRI	Magnetic resonance imaging
DWI	Diffusion-weighted imaging
DSC	Dynamic susceptibility contrast
ADC	Apparent diffusion coefficient
rCBV	Cerebral blood volume ratio
rCBF	Cerebral blood flow ratio
MTT	Mean transient time
TTP	Time to peak
FOV	Field of view
TE	Echo time
TR	Repetition time
ROI	Region of interest
PWI	Perfusion-weighted imaging
GBM	Glioblastoma multiform
SPSS	Statistical package for social sciences

Acknowledgements
Not applicable.

Author contributions
MM and MH designed the research. MH performed the research; and wrote the manuscript. MM (15 years' experience of neuroradiology) and MM (10 years' experience of neuroradiology) analyzed the collected data. MM and MM revised data and manuscript. All authors read and approved the final manuscript.

Funding
Not applicable (no funding received for this study).

Availability of data and materials
Available on request with the corresponding author.

Declarations

Ethics approval and consent to participate
This study was approved by the research ethics committee of the Radiology Department of the Faculty of Medicine Mansoura University on 11/10/2020, Reference number of approval: MS.20.10.9. All patients included in this study gave a written informed consent to participate in the research.

Consent for publication
All patients included in this study gave a written informed consent to publish the data contained in this study.

Competing interests
The authors declare that they have no competing interests.

Received: 1 October 2022 Accepted: 6 January 2023
Published online: 18 January 2023

References

1. Somes J (2019) The top 10 pitfalls to avoid when caring for the older adult: part I. J Emerg Nurs 45(5):576–578
2. Morales KA, Arevalo-Perez J, Peck KK, Holodny AI, Lis E, Karimi S (2018) Differentiating atypical hemangiomas and metastatic vertebral lesions: the role of T1-weighted dynamic contrast-enhanced MRI. Am J Neuroradiol 39(5):968–973
3. Liu X, Tian W, Kolar B, Yeaney GA, Qiu X, Johnson MD et al (2011) MR diffusion tensor and perfusion-weighted imaging in preoperative grading of supratentorial nonenhancing gliomas. Neurooncology 13(4):447–455
4. Essig R, Kuflik E, McDermott SD, Volansky T, Zurek KM (2013) Constraining light dark matter with diffuse X-ray and gamma-ray observations. J High Energy Phys 2013(11):1–29
5. Petrella JR, Provenzale JM (2000) MR perfusion imaging of the brain: techniques and applications. Am J Roentgenol 175(1):207–219
6. Neil J (2008) Diffusion imaging concepts for clinicians. J Magn Reson Imaging Off J Int Soc Magn Reson Med 27(1):1–7
7. Bammer R, Fazekas F, Augustin M, Simbrunner J, Strasser-Fuchs S, Seifert T et al (2000) Diffusion-weighted MR imaging of the spinal cord. Am J Neuroradiol 21(3):587–591
8. Schaefer PW, Grant PE, Gonzalez RG (2000) Diffusion-weighted MR imaging of the brain. Radiology 217(2):331–345
9. Tanenbaum TJ, Williams AM, Desjardins A, Tanenbaum K (2013) Democratizing technology: pleasure, utility and expressiveness in DIY and maker practice. In: Proceedings of the SIGCHI conference on human factors in computing systems
10. Reese TG, Benner T, Wang R, Feinberg DA, Wedeen VJ (2009) Halving imaging time of whole brain diffusion spectrum imaging and diffusion tractography using simultaneous image refocusing in EPI. J Magn Reson Imaging Off J Int Soc Magn Reson Med 29(3):517–522
11. Liu E, He W, Yan CR (2014) 'White revolution'to 'white pollution'—agricultural plastic film mulch in China. Environ Res Lett 9(9):091001
12. Alexander LV, Zhang X, Peterson TC, Caesar J, Gleason B, Klein Tank A et al (2006) Global observed changes in daily climate extremes of temperature and precipitation. J Geophys Res Atmos. https://doi.org/10.1029/2005JD006290
13. Al-AbdulJabbar A, Elkatatny S, Mahmoud M, Abdelgawad K, Al-Majed, (2019) A robust rate of penetration model for carbonate formation. J Energy Resour Technol 141(4):1–9
14. Hasan DI, Abowarda MH, Taha MM (2016) Diffusion-weighted MRI and apparent diffusion coefficient value in assessment of intra-medullary spinal cord masses. Egypt J Radiol Nucl Med 47(4):1575–1584

Publisher's Note